PAPER

Design and assessment of a flexible fish robot actuated by shape memory alloys

Bioinspiration & Biomimetics

PAPER

Design and assessment of a flexible fish robot actuated by shape memory alloys

RECEIVED
21 December 2017

REVISED
27 June 2018

ACCEPTED FOR PUBLICATION
3 July 2018

PUBLISHED
31 July 2018

William Coral[1,2,3], Claudio Rossi[2], Oscar M Curet[3] and Diego Castro[4]

[1] Department of Mechatronics Engineering, Corporación Universitaria del Huila, Huila, Colombia
[2] Centre for Automation and Robotics, Universidad Politécnica de Madrid-CSIC, Madrid, Spain
[3] Department of Ocean and Mechanical Engineering, Florida Atlantic University, Boca Raton, FL, United States of America
[4] School of Engineering, Pontificia Universidad Javeriana, Bogota, Colombia

E-mail: william.coral@corhuila.edu.co

Keywords: shape memory alloys, smart materials, fish-like robot, soft robotics, underwater robotics, locomotion

Supplementary material for this article is available online

Abstract

In this paper, we present a fish-like underwater robot inspired by the black bass fish. This robot is composed of a deformable structure and muscle-like linear actuators based on shape memory alloy wires. Such actuators are used to bend a continuous structure representing the backbone of the fish. The prototype is also equipped with a bio-inspired synthetic skin made of liquid silicone rubber and Lycra microfiber mesh. We present the mechatronics of the prototype and its control scheme, which take advantage of flex sensors for *proprioception*. Experiments under different conditions (in air and in water) assess the effectiveness of the mechatronics design and demonstrate that a relatively simple PID controller provides high precision of the muscles' position control. Here, the implementation of biomimetic kinematics and silent actuation technology in bio-inspired underwater robotics are demonstrated. Progress in this technology could provide multiple applications, including fish farming, coastal protection and live animal monitoring where silent robotics are necessary.

1. Introduction

Over the last few years, the development of bio-inspired and bio-mimetic robotic mechanisms has been emerging in the field of robot modeling, design and control. In particular, fish-like robots have attracted the attention of many researchers. In fact, fishes are capable of high performance movements in water, and designs based on the mechanism of fish biomechanics appear to be a promising alternative for underwater robots.

Fish-like robots show intriguing potential, including fish farming, coastal monitoring and surveillance, among others. While land-based autonomous robots have already made a significant breakthrough in markets related to service robotics, including the agro-alimentary sector, robotics and advanced information technology tools are still underdeveloped in the fisheries sector. The introduction of this kind of robot in this industry will allow us to address topics such as robot–animal interaction in order to reduce its impact on the stress of the animals, but also to induce specific behaviors in the fish [1, 2]. In fact, besides applications such as *in situ* continuous water quality monitoring and fish observation, induced swimming behaviors are being considered in order to improve fish wellness, with a direct repercussion on production costs and food quality, not forgetting animal welfare ethical issues [3, 4]. For this reason, carefully designed bio-inspired swimming patterns and innovative silent actuation technology will be beneficial.

A fair amount of work developing underwater robots inspired by the swimming mechanism of fishes can be found in the literature, adopting a variety of actuation technologies and mechanical setups [5].

A large number of robotic fishes are based on classic mechatronic systems (DC motors or servomotors). Full-body undulatory swimming, where the fish body is a structure made of a discrete number of rigid elements actuated by servomotors, is proposed in [6, 7]. Fin-based propulsion has also been proposed. Propulsion can be generated by an oscillating caudal fin, moved by servomotors [8] or DC motors [9]. In particular, [9] focusses on the study of various parameters, such as oscillation frequency and amplitude as well as aspect ratio and the rigidity of the caudal fin. An origi-

nal fin-based locomotion and maneuvering system is proposed in [10] based on the knifefish. This fish has a unique swimming system based on its ribbon-like anal fin. The robotic knifefish is provided with a similar ribbon-like fin, actuated by a set of DC motors. An alternative use of DC motors is adopted in the MIT fish [11], which is composed of a continuous soft body, where a signal is used to produce a wave that propagates backwards along the body in order to generate propulsion.

Pneumatic actuation has been adopted in the *Airacuda* robot by *FESTO* that uses pneumatic artificial muscles, and in the *SoFi* fish [12], that employs soft fluidic actuators to generate cyclic hydraulic flows for the actuation of an undulating soft structure representing the body of the fish.

The use of functional materials, such as electro-active polymers, piezo-electric fiber composites and shape memory alloys (SMAs), provide promising alternatives to standard servomotor technology, since they allow lighter, simpler and smaller robots to be built that could be used for animal–robot interaction. Electro-active polymer-based fishes mostly rely on the use of ionic polymer–metal composites (IPMC) for building hydrofoils (see, for example, [13, 14]). Such robots display *carangiform* swimming: a passive tail is undulated by an oscillating IPMC beam representing the rear part of the fish body. SMA wires for actuation have been used for bending soft structures embedded into an elastic material such as silicone [15–18] or used as linear actuators in articulated structures [19–21]. Piezo-ceramic actuators are also used in different prototypes. In the robot proposed in [22], the whole fish body is composed of an oscillating piezoelectric fiber composite plate. In [23, 24], the tail fin is actuated by a piezoceramic composite actuator.

In recent work, we used SMAs as actuation technology due to their advantages in being able to work with a wide range of electrical currents from 45 mA–4000 mA [25, 26], their excellent mechanical characteristics (force-to-mass ratio), low price and commercial availability. SMAs are generally considered unsuitable for robotic applications due to their slow actuation speed and because they are difficult to control, since their actuation is non-liner and shows hysteresis. This is based on the fact that the SMA's response speed is limited due to slow heat transfer characteristics and the long transient associated with the phase transformation process. Nonetheless, we have shown [27, 28] that SMAs can effectively be used as actuators in robotics using proper control and mechanical design. Actually, it has been demonstrated that NiTi SMA wires can be surprisingly fast and precise [29, 30].

In previous work [27, 31], we have presented the first laboratory prototype of a bio-mimetic underwater robot, the *iTuna*, that has a continuous structure mimicking the backbone of the fish (*notochord*), and the use of SMAs as *red muscles* to bend the body of the fish. Here, we present a new design based on the same principle, but with significant improvements in the mechatronics design and control algorithms, such as actuation speed, structural integrity and construction difficulty. Simulations were performed in order to design the fish, and extensive experiments were conducted to demonstrate its performance.

The motivation for our work is to gradually close the gap between labwork and actual commercial applications in the agro-alimentary sector. The prototype (which we refer to as 'BR3') was modeled according to the physical characteristics of the sea bass because it is the second largest production volume in Mediterranean fish farming.

The paper is organized as follows. Section 2 describes the mechanical design of the proposed system, and section 3 describes the control hardware and software designed. Section 4 reports the results of the experiments conducted to assess the performance of the system, and a conclusion is presented in section 5.

2. Mechanical design

Fish swim in a number of different ways. Here, we focus on body and/or caudal fin locomotion. In this kind of swimming, the fish undulates its body producing a backward-propagating propulsive wave. According to the wave length, compared to the body length, and to the way the thrust is generated, swimming is classified by a range of swimming modes: *anguilliform*, *subcarangiform*, *carangiform* and *thunniform*. The sea bass exhibits a carangiform swimming mode, which means that body undulations are confined to the last third of the body length (see [32, 33]).

Ideally, in order to propagate such a wave along the body, a continuous body is needed. In robots, this is approximated by a relatively small number of rigid segments. Unlike most robotic fishes, the design presented here consists of a continuous flexible body. Hence, the waveform is approximated by arcs of circles instead of segments, allowing a good approximation of the subcarangiform, carangiform and thunniform swimming modes, even with only two elements (see [27]).

The main component of the robot is a continuous structure made of 1 mm thick polycarbonate representing the fish backbone and spines and giving support to the body and electronics parts (figure 1). This material was chosen for its flexibility and temperature resistance, since SMAs can heat up to 90 °C. The designed backbone of the fish has a length of 263 mm, similar to the length scale of juvenile sea bass.

The backbone has two rectangular holes where the SMAs are located. In this way, the effective cross section of the polycarbonate structure is reduced by approximately 50% with respect to the previous designs. This reduces its resistance to bending and optimizes the pull force on the SMA. Additionally, it prevents the external SMA wires from being over-

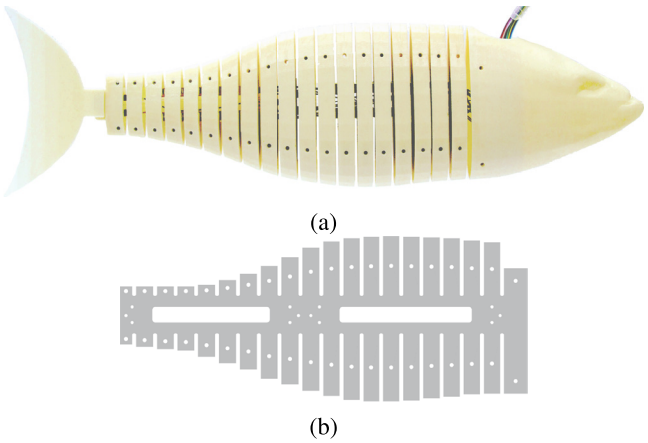

Figure 1. (a) Real BR3 prototype without skin. The whole body was printed using ABS plastic. It is composed of 19 ribs, a rigid caudal fin, and head. (b) Continuous flexible 1 mm-thick polycarbonate backbone. The SMA wires, SMA drivers, current, flex and temperature sensors are attached to the backbone.

stretched by the backbone when the structure bends. Such over-stretching causes slack in the SMAs after functioning for some time, which in turn causes a loss in the bending angles obtained: the SMAs only contract approximately 4% of their length, so even very small slack in their functioning has a significant impact on the overall performance.

The backbone beam also includes 20 *spines* that are used to support the robot's body. This is made up of a set of 20 solid sections made of ABS plastic which we refer to as *ribs*[5]. Based on our previous experience, we adopted a high number of solid sections to increase the mass of the fish and to provide a better skin support in order to obtain smoother body curves. The last factor was found to be key to reducing water flow perturbations and vorticity.

2.1. Actuation

The backbone of the fish is divided into two sections of different lengths. Each section has two antagonist SMA wire actuators attached that, when powered, bend the corresponding section of the backbone. The SMA wires are 234 mm and 212 mm long and are arranged in a V-shaped configuration (figure 1) in order to double the pull force. This arrangement achieves a maximum bending of approximately 38 degrees, regardless of the fact that SMA wires only contract by a maximum of 4% of their length. The diameter of the SMA wires adopted is 0.15 mm, which provides a good trade off between current consumption (410 mA nominal), and pull force (321 g). The cooling time is 1.7 s when the wire is heated to 90 °C. By using currents higher than 410 mA, the contraction time can be reduced at the cost of inducing fatigue (resulting in a reduced strain) in the actuator after some operation time (see [28]).

[5] Most fishes do not actually have ribs. This term is used here only figuratively.

2.2. Ribs

The entire fish was designed based on a 3D model from a real bass reproduced in the *Autodesk Inventor*® CAD software.

For simulation purposes, we exported the model from *Autodesk Inventor*® to *MATLAB*® using the *SimMechanics*™ toolbox. The fish body was simulated with 20 rigid segments similar to the physical model, connected by primitive joints with one rotational degree of freedom of the same length of the ribs. The flexible structure was not included in the simulations due to the limitations of the software. Figure 3 shows the simulated model.

Using the CAD model, we estimated the maximum rotational angle for each section for various ribs thicknesses, inter-rib space and number of ribs, as shown in figure 3. Note that in order to allow to the movement of the SMAs inside the fish, the inner section of each rib must be partially hollow (figure 3, right). Examples of the rib dimensions are shown in table 1. The last section (rib number 20) is used as a dock to attach different caudal fins.

The capability of reproducing different swimming kinematics was verified with the computational model. Figure 4 shows some stills of three swimming modes.

2.3. Skin

The entire robot fish, except its head, is covered with a synthetic skin. The physical characteristics of this skin make it one of the most complex parts of the fish design. It must satisfy three main objectives. The first, *mobility*, refers to the robot being able to bend his body without resistance. Clearly, the induced resistance in the fish movement due to the skin effect should be as small as possible. For a good *mobility*, the elasticity is the most important characteristic of the material used. The second objective is *impermeability* to protect all the electronic components (sensors, batteries and actuators). Water impermeability is the most

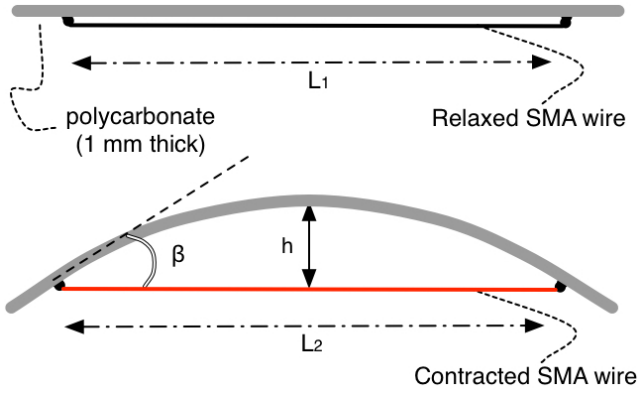

Figure 2. Principle of the bendable structure. An SMA wire runs parallel to the backbone segment. As the SMA contracts, it causes the polycarbonate backbone to bend (angle β and height h). L_1 is the length of the relaxed SMA and L_2 is the length of the contracted SMA.

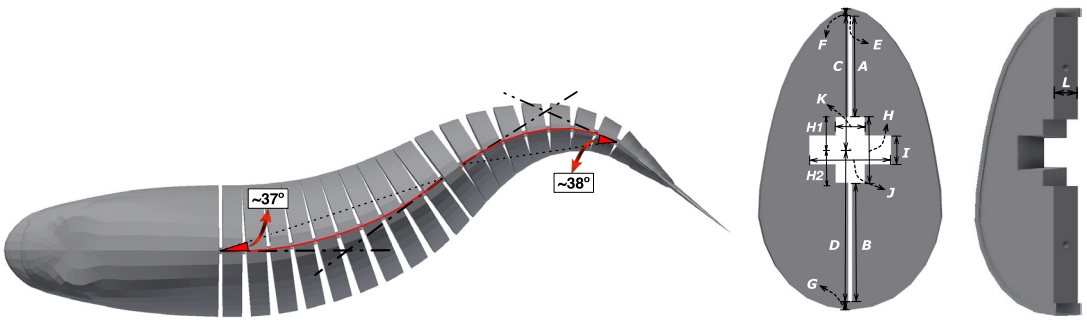

Figure 3. Simulated BR3 in SimMechanics. Right: top view. The red line represents the backbone, while the dotted black lines represent the contracted SMAs. The angles shown relate to the number and thickness of the ribs, inter-rib spaces and SMA length when contracted. Left: rib (see also table 1).

Table 1. Examples of rib sizes (rib numbers 7 and 20).

Section number/ dimension	A	B	C	D	E	F	G	H	H1	H2	I	J	K	L
7	38	43.5	50.5	56	1.5	3.331	4.469	25	12.5	12.5	11	31	11	10.5
20	6	7	18.5	19.5	1.5	3.557	2.559	25	12.5	12.5	11	12	11	8

Note. Measurements are in millimetres (mm).

important characteristic of the material used for the skin, and also when the material is stretched. The third objective refers to *durability*, i.e. mechanical resistance.

We tested a variety of materials and techniques in order to produce a skin with good values for the three parameters described above. Three different materials (latex, liquid silicone rubber[6] and rubber paint[7]) were used to produce a protective (waterproof) layer. However, these materials by themselves could not reach the impermeability target because, after some stretching, they allow water to leak in at the location where the skin and main body are attached. A way to solve this problem is to increase the amount of layers applied, at the cost of reducing the elasticity and thus affecting skin mobility.

The results of these early tests highlighted the importance of including a material that serves as support for the protective material[8]. Such a 'carrier' material should provide the function of preventing the formation of holes in the external layer, preventing localised over-stretching, and helping to provide a more uniform distribution of the protective material. Furthermore, it helps to give the skin a specific shape.

Biological skin consists of two layers (epidermis—outer layer and dermis—internal layer), plus a hypodermic subcutaneous layer [35]. The epidermis has a

[6] *Dragon Skin*® 10 medium, high performance silicone rubber.

[7] *Plasti — Dip* multi-purpose rubber coating aerosol spray.

[8] This idea emerged from a conversation with some colleagues during the Workshop on Bio-Inspired Robots, Nantes, France, 2011. Regrettably, we do not know their names and cannot, therefore, give them proper credit.

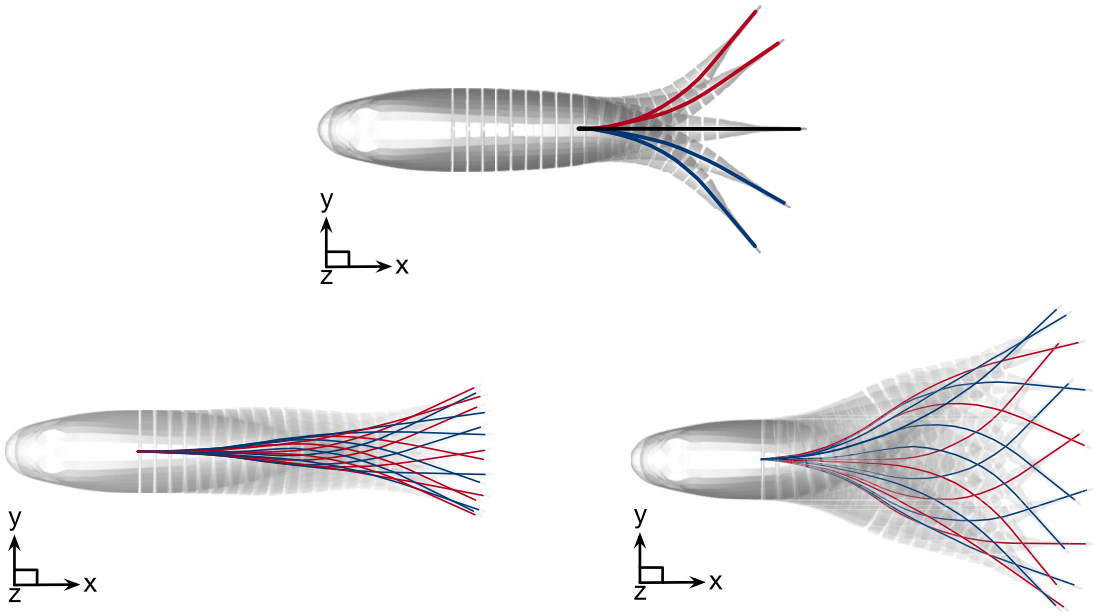

Figure 4. Axial view of the simulated swimming modes: thunniform, carangiform and subcarangiform. Each line of the simulated swimming mode was traced along the body to prove that the BR3 was capable of mimicking these three swimming modes [33, 34]. The maximum amplitude reached for each undulatory locomotion was 22.5 cm (thunniform), 13 cm (carangiform) and 29 cm (subcarangiform).

protective function, while the dermis has a structural function, giving support, density and strength to the epidermis.

In a similar fashion, we designed a synthetic skin which is composed of two main components: a structural component and a protective component. As a carrier component (dermis), we adopted a Lycra microfiber mesh (LMM) due to its flexibility (so it does not affect mobility) and mechanical resistance (enhanced durability) and because it allows a good adherence of the protective component (latex, liquid silicone and rubber paint). Using such a substrate, we again tested the three protective components mentioned earlier (representing the epidermis). A sample of the 'silicone rubber skin tissue' can be seen in figure 5.

Table 2 shows a qualitative comparison between the six resulting skin models. Note that the tests carried out for the parameters of *mobility* and *durability* for the case of *rubber paint* report N/A (not applicable) because, due to its rigidity, the skin did not stretch at all.

3. Modeling and control

3.1. Electronics

SMAs can be used as both actuators and sensors at the same time as their resistance changes with contraction. This attribute can be advantagous when controlling the kinematics of a robotic fish [27, 28]. In fact, when SMAs contract, their resistance changes. Thus, the measure of the resistance can be directly related to their length, and can be used for position control. Resistance measures can be obtained indirectly by measuring the current consumption of the SMAs.

Here, we equipped the prototype with flex sensors (see figure 1) to obtain a more precise angle measurement. These provide a less noisy signal with respect to the current sensors. Also, since the range of resistance changes is very small (the order of $\mu\Omega$), a very precise analog-to-digital converter was needed (a 12 bit A/D was used in the *iTuna*), while with the flex sensors, an 8 bit A/D was sufficient. Current sensors were also used in the BR3 as a safety measure to prevent high currents in the SMAs and to avoid damaging them. A temperature sensor was used to measure the temperature inside the whole body; however, this measurement was not used in the control system. In future works, we will consider the effect of temperature on the performance of the robot.

3.2. System modeling

The control accuracy of the SMA actuators is difficult due to their inherent hysteresis and non-linearities with local memory, resulting from the influence of previous behavior. In addition, further hysteresis behavior will manifest while operating the SMA inside their natural hysteresis zone as a result of the local memory described before. The 'inside' hysteresis that the SMA presents is smaller but much more complex, which presents a major challenge for any mathematical modeling of the phenomena and a theoretical approach to the controller design.

Nonetheless, to control the SMA, it is very important to have a dynamic model of the SMA plant involving the relationship between the observed output to

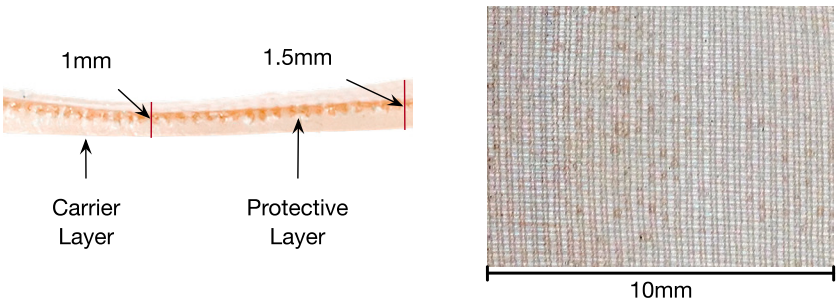

Figure 5. Sample of silicone rubber skin tissue. As the skin was hand made, the thickness varies between a minimum of 1 mm and a maximum of 1.5 mm along the entire skin.

Table 2. Comparison chart between the materials used for the skin.

Parameters material	Mobility	Impermeability	Durability
Latex			
Rubber paint	N/A		N/A
Liquid silicone			
Latex & LMM			
Rubber paint & LMM	N/A		N/A
Liquid silicone & LMM			

Note.  = Good,  = Better,  = Best.

the specified input. An SMA input power to output bend model, in terms of a transfer function, has been obtained experimentally for each SMA. Figure 6 shows the input signals used for identification and the output signals obtained, where the left column shows the input signals (duty cycle) and the right column shows the output signals (bend ratio measured in degrees).

Using this experimental data, the transfer functions were obtained using the system identification toolbox *Ident* of MATLAB®. We considered three candidate transfer functions, finding the parameter that best fitted the experimental data. For each transfer function, we measured the difference between the simulated response of the model and the measured data (table 3). As a final model, we selected the 3 poles—1 zero configuration because the increased complexity of the 3 poles—2 zeros configuration did not show a significant increase in the normalized root mean square error between the model and the data.

The final transfer function obtained for each pair SMA-flex sensor was as follows:

$$STL(s) = \frac{895.2s+169.9}{s^3+7.356s^2+4.896s+0.5717} \quad \text{SMA wire Tail Left (STL)} \tag{1}$$

$$STR(s) = \frac{358.1s+8532}{s^3+8.939s^2+89.41s+69.19} \quad \text{SMA wire Tail Right (STR)} \tag{2}$$

$$SHL(s) = \frac{429.1s+459.7}{s^3+6.055s^2+9.526s+3.279} \quad \text{SMA wire Head Left (SHL)} \tag{3}$$

$$SHR(s) = \frac{741.9s+69.01}{s^3+7.118s^2+6.128s+0.5014} \quad \text{SMA wire Head Right (SHR).} \tag{4}$$

3.3. Controller setup

For the control strategy, we used a PID controller. Using the Ziegler–Nichols methodology, we tuned the proportional, K_p, integrative, K_i, and derivative, K_d, of the PID controller based on the analysis of the system under both opened/closed loops. The system was represented by the identified model in equations (1)–(4). The PID configuration was parallel given the following equation, (equation (5)),

$$C_{\text{PID}}(s) = K_p + K_i\frac{1}{s} + K_d s. \tag{5}$$

The PID tuning for the four SMAs was performed imposing the same settling times for all of them. This

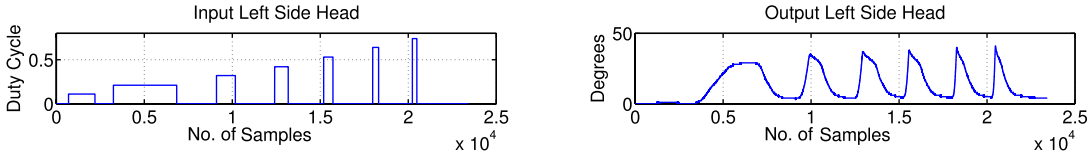

Figure 6. Example of the input/output signals used for system identification (left/head SMA). The input signal is in the form of a pulse width modulated (PWM) signal, the output is measured as the value of the bending angle β. Time (x axis) is measured in the number of samples (100 samples s^{-1}).

Table 3. Fit to estimation data (normalised root mean square error).

Poles, Zeroes	STL (%)	STR (%)	SHL (%)	SHR (%)
2, 1	62.64	66.85	59.96	53.97
3, 1	65.17	66.85	63.64	68.3
3, 2	74.03	66.99	73.98	63.45

was done because it is critical to have the same time response in the SMAs in the antagonistic configuration and to prevent a singularity configuration. Table 4 shows the values for each gain K_p K_i and K_d, the performance and robustness parameters.

As we can see in equation (2) and table 4, there were significant differences between the STRs transfer function, PID parameters and the others. These differences could be explained by accidental overheating of the SMA in early testing, the age of the SMA or quality differences in the production process.

3.4. Control schema

The control scheme is based on two main parts, a high level planner which selects the bend set point as a time function depending on the swimming mode that the fish would have to follow, and the second part is a low level PID-based position controller which uses the flex sensor to adjust the duty cycle of the pulse width modulated (PWM) current signal that drives the SMA, its input. Figure 7 shows the closed-loop control block diagram.

The input of the whole system is a desired tail tip angle which follows a time variant function dependent on the equivalent biological counterpart. This high level planner inputs the bend set point to the low level controller, which is a time variant signal. The output signal of the PID controller passes through a dynamic current limiter to avoid any over current damage to the SMA wire, and the maximum current changes according to the present condition of the SMA. The output of the limiter is the input of the power drive of the wire, being the wire actuator. The feedback of the signal is a current sensor to adjust the limiter maximum and the flex sensor signal. The former signal is the feedback to the PID controller from which it calculates the error to perform the control. Both signals are analog, which require an analog-to-digital converter to interact with the rest of the control system. This conversion makes necessary the selection of a working frequency; in this case it was set to 333.33 Hz to avoid aliasing, harmonics or sampling issues.

4. Experimental results

We tested the prototype in three different situations in order to compare the real behavior with respect to the theory and the simulations. In all situations, the fish was fixed by the head. Figure 8 shows the experimental setup in the three cases. To determine the trajectory of each reference spot, a particle tracking visualization was made. Reference marks were located at the end of the first body segment and at the tail tip (figure 8(b)). A camera was located over the fish tail (looking downwards). A video (available online at stacks.iop.org/BB/13/056009/mmedia) was recorded at 60 frames per second.

In the three situations, the difference amplitude and frequencies of the oscillations were tested. In the following figures, we provide examples of the results obtained for various oscillation frequencies and amplitudes. In all plots, the red line is the reference signal, and the blue line is the result of the tracking of the tail tip. The tested swimming mode was the carangiform.

To evaluate the performance of the prototype, the fish was tested in the following configurations: (1) only with the backbone (no ribs or skin); (2) backbone and ribs (no skin); (3) backbone, ribs and skin; and (4) the same elements as (3) but inside the water. This addition of components (ribs and skin) increases the overall maximum performance available for the experiments, allowing faster actuation's and wider angles. This increase in performance is due to these elements increasing the damping effect on the whole body and reducing the oscillations at the desired reference angle. Finally, changing the experiment environment to water decreases the cooling time of the SMAs, which further increases the maximum actuation frequency of the fish.

4.1. Air, backbone only

This first set of experiments (see figure 8(a)) was made in order to test the system and to provide a baseline that allows us to identify the effects of the extra weight and the tensile strength produced by the ribs and skin, respectively. These experiments where performed at half (0.34 Hz) the maximum theoretical frequency and a very low frequency (0.116 Hz), ensuring safe operation. Since the controller was tuned up considering the

Table 4. PID controller characteristics.

SMA	K_p	K_i	K_d	Rise time (s)	Settling time (s)	Overshoot (%)	Peak
STL	1.1442	1.8628	0.159 74	0.0155	0.0271	0.116	1
STR	78.7223	618.4335	2.5052	0.002 15	0.0271	4.3	1.04
SHL	1.6841	2.1174	0.334 85	0.0153	0.0271	0	1
SHR	1.3619	2.1995	0.193 87	0.0153	0.027	0.0165	1

Note. For all the systems, closed-loop stability is obtained.

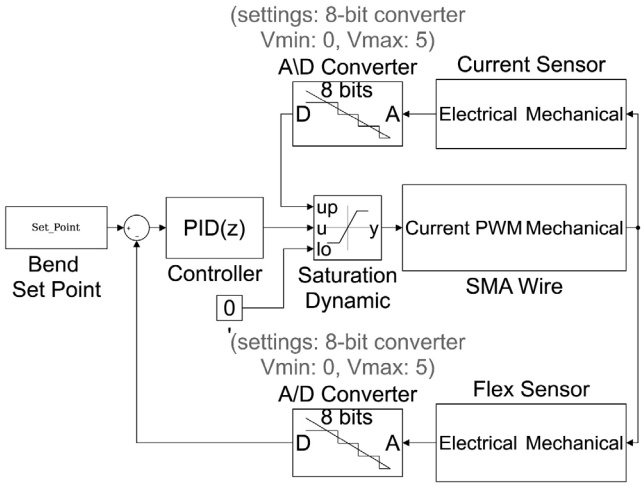

Figure 7. Low-level position control loop for a single SMA actuator. Each one includes the set point, the discrete PID controller implemented on the microcontroller, the ADC and the dynamic saturation block. Table 4 and equations (1)–(4) describe the system and the controller.

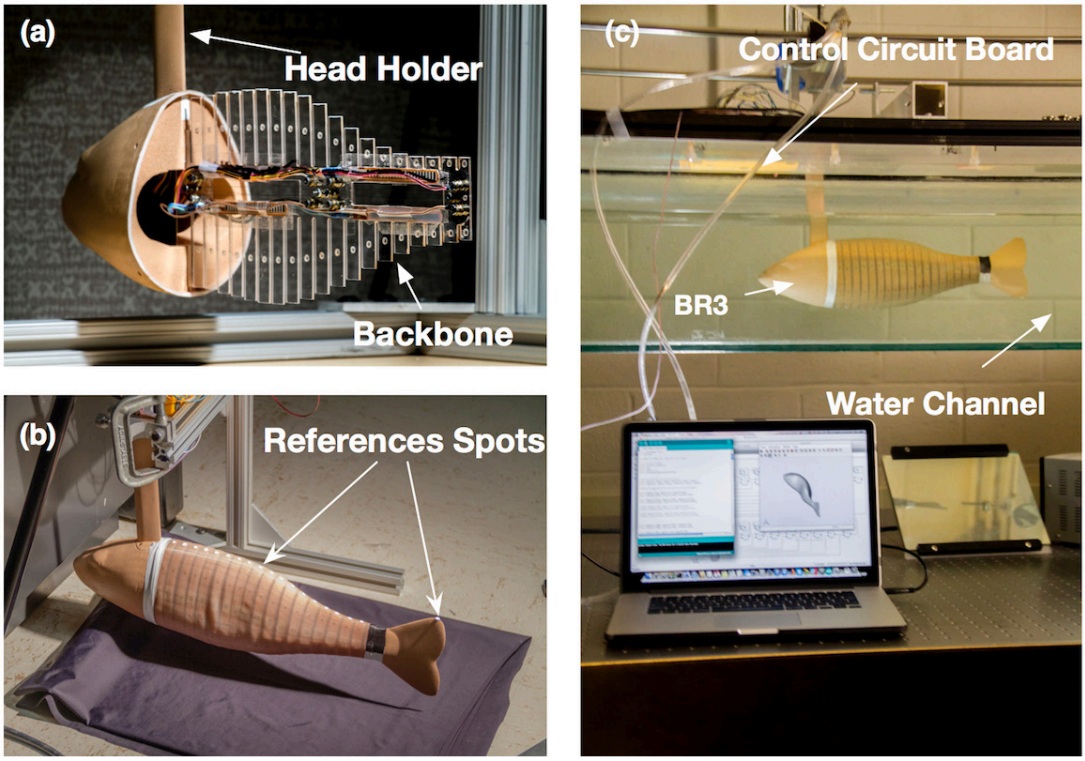

Figure 8. Experimental testbed: (a) air, backbone only; (b) air, backbone+ribs+skin; (c) water, backbone+ribs+skin.

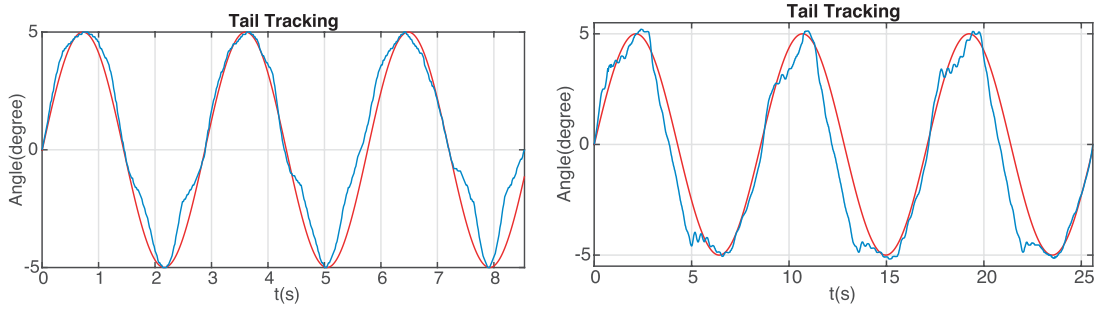

Figure 9. Trajectory of the tail tip in air (backbone only). Left: frequency =0.34 Hz; right: frequency = 0.116 Hz.

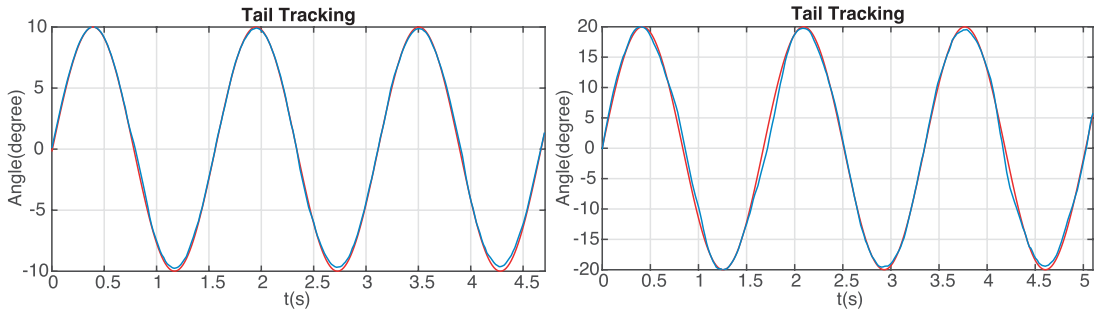

Figure 10. Trajectory of the tail tip in air (whole body, backbone and ribs and skin).

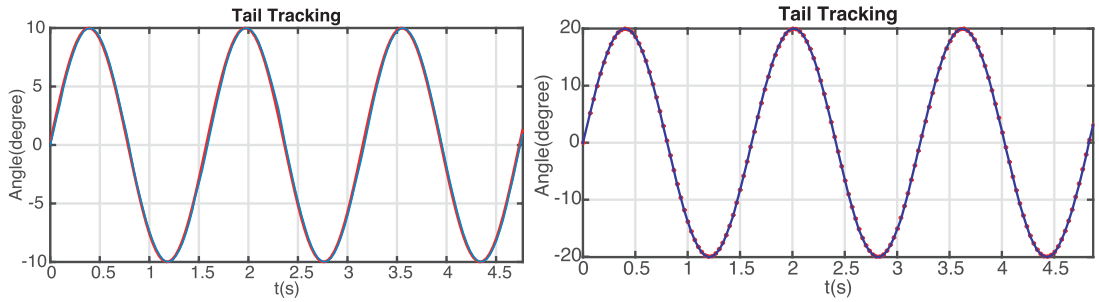

Figure 11. Trajectory of the tail tip in water (whole body).

dynamics of the whole body (ribs and skin), these experiments were expected to provide relatively poor results. Nonetheless, they were useful in determining the maximum frequency of the oscillation achievable without added mass and without skin, which had been 0.65 Hz. This is approximately 10% higher than the theoretical maximum frequency achievable according to the nominal cooling time of the SMA of 1.7 s, meaning a maximum frequency of 0.588 Hz.

Figure 9 shows an example of the accuracy of the control with respect to the reference signal (in red). The reference position was set to 5° for both sections. This angle was chosen to maintain a safe operation of the SMAs due to the absence of ribs and skin in this experiment.

4.2. Air, backbone and ribs and skin

In the second set of experiments, the ribs and skin were added to the backbone, forming the complete robot. Figure 8(b) shows the experimental setup. Figure 10 shows the desired and output kinematics, including the backbone, ribs and skin in air for oscillating angles of 10° and 20° for both sections, and for the maximum frequency achieved in the first test (approximately 0.65 Hz). Notice that the robot is able to follow the trajectory much more closely in this experiment. This is because, during the controller tuning, the whole system's dynamics was considered, including the effects of water and skin, which works as a 4 order spring-dampener system. During these experiments, the controller shows that it can work even missing the dampening effect of the water and managing to follow the planned trajectory within an error of 10%.

[9] ATI Industrial Automation, www.ati-ia.com; Measurement Computing, www.mccdaq.com; National Instruments, www.ni.com

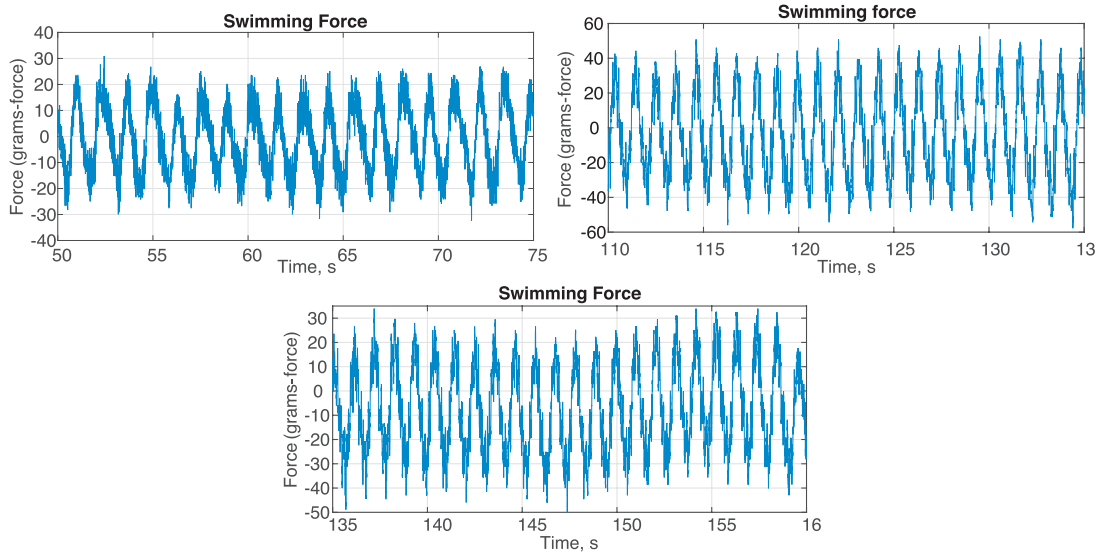

Figure 12. Tail flapping force measured during water channel tests. Top, left: $f = 0,65$ Hz, amplitude $= 20°$; top, right: $f = 1$ Hz, amplitude $= 20°$; bottom: $f = 1$ Hz, amplitude $= 10°$.

4.3. Water, backbone and ribs and skin

The last set of experiments was performed with the complete robot underwater. The tests were performed using the water tunnel in the Hydrodynamic Lab at Florida Atlantic University. The complete setup is depicted in figure 8(c). These experiments were performed in still water (no water flow).

In these experiments, the fish was attached to a Nano 17 transducer to measure the force response through a data acquisition device (DAQ) USB-1208FS and a data acquisition card (NI-DAQ) NI PCI-6220[9]. The transducer has a resolution of 0.318 gram-force. The sensor calibration information is provided in the appendix.

It was found that there was a good agreement between the desired and output kinematics of the robotic fish (see figure 11). The controller showed an excellent performance: the mechatronics design demonstrated an ability to perform the same in water as in air, as far as position control is concerned.

Finally, we measured the tail flapping force produced by the fish during swimming. In these experiments, we increased the oscillation frequency up to 1 Hz (see figure 12). Note that, according to the maximum theoretical frequency of 0.588 Hz (nominal cooling time), the antagonistic SMA setup and control were able to achieve a speedup of approximately 70%.

Figure 12 shows the tail flapping force obtained during the experiments at $f = 0.65$ Hz and $f = 1.0$ Hz and with amplitudes of the oscillation of the tail tip of 10° and 20°.

It can be noticed that a higher actuation frequency produces a higher tail flapping force for the same amplitude of the oscillation of the tail tip. Also, it can be observed that at a flapping frequency of 1.0 Hz and a maximum tail degree of 10°, the tail flapping force produced is almost double compared to the flapping force when the amplitude of the oscillation of the tail tip is 20° with the same actuation frequency.

5. Conclusions

In this paper, we presented the design and control of a silent bio-inspired robotic fish that uses antagonistic SMAs for actuation. The robotic fish features a continuous flexible backbone, a series of 3D printed body segments and self-contained electronics and sensors to control the kinematics. A three-dimensional computational model was used to evaluated the dynamics and kinematics of the robotic system. A series of experiments using the robotic model under different conditions were conducted and compared against the computational model. The results show a good agreement between the simulated conditions and the experiments.

This work has shown that relatively simple PID controllers can achieve an excellent performance for the actuation control bio-inspired fish kinematics. The progress of quite actuators in the control of continuous flexible bodies will be a key factor in numerous applications, including fish farming, surveillance and coastal monitoring.

Acknowledgments

This work has been partially funded by the RoboCity2030-III-CM project (S2013/MIT-2748), funded by the *Programas de Actividades I + D en la Comunidad de Madrid* and co-funded by the Structural Funds of the EU. The first author acknowledges the support of the Administrative Department of Science, Technology and Innovation ('COLCIENCIAS', grant call 568 2013) and of the Foundation for the Future of Colombia ('COLFUTURO', grant call 2012) of Colombia.

Appendix. Sensor calibration data

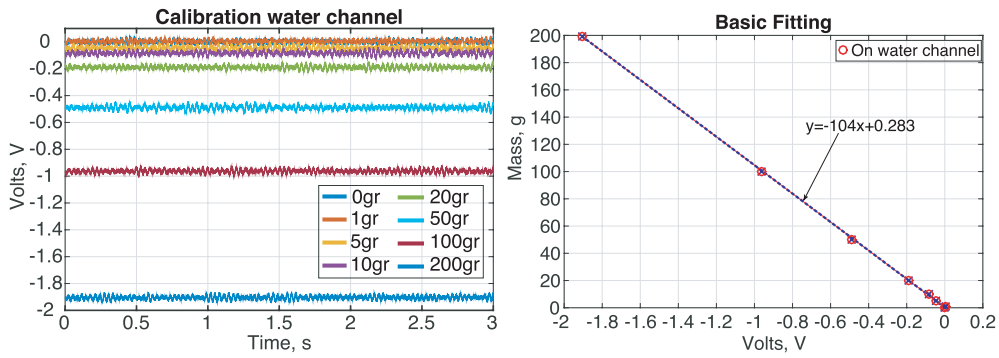

Figure A1. Force sensor calibration. Left: raw data; right: fit curve.

ORCID iDs

William Coral https://orcid.org/0000-0002-3971-9536
Claudio Rossi https://orcid.org/0000-0002-8740-2453
Oscar M Curet https://orcid.org/0000-0002-3202-6841
Diego Castro https://orcid.org/0000-0003-0022-8868

References

[1] Butail S, Abaid N, Macrì S and Porfiri M 2015 *Fish–Robot Interactions: Robot Fish in Animal Behavioral Studies* (Berlin: Springer) pp 359–77
[2] Bartolini T, Mwaffo V, Showler A, Macr S, Butail S and Porfiri M 2016 Zebrafish response to 3d printed shoals of conspecifics: the effect of body size *Bioinsp. Biomim.* **11** 026003
[3] Rossi C, Coral W and Barrientos A 2013 Robotic fish to lead the school *Swimming Physiology of Fish: Towards Using Exercise to Farm a Fit Fish in Sustainable Aquaculture* ed P Arjan Palstra and V Josep Planas (Berlin: Springer) pp 407–21
[4] Herbert N A 2013 Practical aspects of induced exercise in finfish aquaculture *Swimming Physiology of Fish: Towards Using Exercise to Farm a Fit Fish in Sustainable Aquaculture* ed P Arjan Palstra and V Josep Planas (Berlin: Springer) pp 377–405
[5] Coral W, Rossi C, Colorado J, Lemus D and Barrientos A 2012 SMA-based muscle-like actuation in biologically inspired robots: a state of the art review *Smart Actuation and Sensing Systems—Recent Advances and Future Challenges* (Rijeka: InTech)
[6] Hu H 2006 Biologically inspired design of autonomous robotic fish at Essex *IEEE SMC UK-RI Chapter Conf. on Advances in Cybernetic Systems* pp 3–8
[7] Anderson J M and Chhabra N K 2002 Maneuvering and stability performance of a robotic tuna *Integr. Comp. Biol.* **42** 118–26
[8] Morgansen K A, Triplett B I and Klein D J 2007 Geometric methods for modeling and control of free-swimming fin-actuated underwater vehicles *IEEE Trans. Robot.* **23** 1184–99
[9] Low K H and Chong C W 2010 Parametric study of the swimming performance of a fish robot propelled by a flexible caudal fin *Bioinspir. Biomim.* **5** 046002
[10] Liu H and Curet O M 2018 Swimming performance of a bio-inspired robotic vessel with undulating fin propulsion *Bioinspir. Biomim.* **13** 056006
[11] Valdivia P, Alvarado Y and Youcef-Toumi K 2006 Design of machines with compliant bodies for biomimetic locomotion in liquid environments *ASME J. Dyn. Syst. Meas. Control* **128** 3–13
[12] Katzschmann R K, Maille A D, Dorhout D L and Rus D 2016 Cyclic hydraulic actuation for soft robotic devices *IEEE/RSJ Int. Conf. on Intelligent Robots and Systems* pp 3048–55
[13] Aureli M, Kopman V and Porfiri M 2010 Free-locomotion of underwater vehicles actuated by ionic polymer metal composites *IEEE/ASME Trans. Mechatron.* **15** 603–14
[14] Shen Q, Wang T, Liang J and Wen L 2013 Hydrodynamic performance of a biomimetic robotic swimmer actuated by ionic polymer-metal composite *Smart Mater. Struct.* **22** 075035
[15] Wang Z, Hang G, Wang Y, Li J and Du W 2008 Embedded SMA wire actuated biomimetic fin: a module for biomimetic underwater propulsion *Smart Mater. Struct.* **17** 25–39
[16] Zhang Y H, Song Y, Yang J and Low K H 2008 Numerical and experimental research on modular oscillating fin *J. Bionic Eng.* **5** 13–23
[17] Wang Z, Wang Y, Li J and Hang G 2009 A micro biomimetic manta ray robot fish actuated by SMA *Proc. of the IEEE Int. Conf. on Robotics and Biomimetics* pp 1809–13
[18] Zhang Z, Philen M and Neu W 2010 A biologically inspired artificial fish using flexible matrix composite actuators: analysis and experiment *Smart Mater. Struct.* **19** 094017
[19] Rediniotis O K, Wilson L N, Lagoudas D C and Khan M M 2002 Development of a shape-memory-alloy actuated biomimetic hydrofoil *J. Intell. Mater. Syst. Struct.* **13** 35–49
[20] Zhang Y, Li S, Ma J and Yang J 2005 Development of an underwater oscillatory propulsion system using shape memory alloy *Proc. of the IEEE Int. Conf. on Mechatronics and Automation* pp 1878–83
[21] Suleman A and Crawford C 2008 Design and testing of a biomimetic tuna using shape memory alloy induced propulsion *Comput. Struct.* **86** 491–9
[22] Ming A, Park S, Nagata Y and Shimojo M 2009 Development of underwater robots using piezoelectric fiber composite *IEEE Int. Conf. on Robotics and Automation* pp 3821–6
[23] Nguyen Q S, Heo S, Park H C and Byun D 2010 Performance evaluation of an improved fish robot actuated by piezoceramic actuators *Smart Mater. Struct.* **19** 035030
[24] Nguyen Q S, Park H C and Byun D 2011 Thrust analysis of a fish robot actuated by piezoceramic composite actuators *J. Bionic Eng.* **8** 158–64
[25] Lambert T R, Gurley A and Beale D 2017 SMA actuator material model with self-sensing and sliding-mode control; experiment and multibody dynamics model *Smart Mater. Struct.* **26** 035004–13
[26] Xiang C, Yang H, Sun Z, Xue B, Hao L, Rahoman M D A and Davis S 2017 The design, hysteresis modeling and control of a novel SMA-fishing-line actuator *Smart Mater. Struct.* **26** 037004–12

[27] Rossi C, Colorado J, Coral W and Barrientos A 2011 Bending continuous structures with SMAs: a novel robotic fish design *Bioinspir. Biomim.* **6** 045005
[28] Colorado J, Barrientos A, Rossi C and Breuer K S 2012 Biomechanics of smart wings in a bat robot: morphing wings using SMA actuators *Bioinspir. Biomim.* **7** 036006
Colorado J, Barrientos A, Rossi C and K S Breuer 2013 Biomechanics of smart wings in a bat robot: morphing wings using SMA actuators *Bioinspir. Biomim.* **8** 019501 (erratum)
[29] Meier H, Czechowicz A and Haberland C 2009 Control loops with detection of inner electrical resistance and fatigue-behaviour by activation of niti-shape memory alloys *European Symp. on Martensitic Transformations*
[30] Teh Y H and Featherstone R 2008 An architecture for fast and accurate control of shape memory alloy actuators *Int. J. Robot. Res.* **27** 595–611
[31] Rossi C, Coral W, Colorado J and Barrientos A 2011 A motor-less and gear-less bio-mimetic robotic fish design *IEEE Int. Conf. on Robotics and Automation* pp 3646–51
[32] Sfakiotakis M, Lane D M and Davies J B C 1999 Review of fish swimming modes for aquatic locomotion *IEEE J. Ocean. Eng.* **24** 237–52
[33] Wen L and Lauder G 2013 Understanding undulatory locomotion in fishes using an inertia-compensated flapping foil robotic device *Bioinspir. Biomim.* **8** 046013
[34] Lauder G V, Lim J, Shelton R, Witt C, Anderson E and Tangorra J L 2011 Robotic models for studying undulatory locomotion in fishes *Mar. Technol. Soc. J.* **45** 41–55
[35] Hawkes J W 1974 The structure of fish skin *Cell Tissue Res.* **149** 159–72